Sodium channel dysfunction in intractable childhood epilepsy with generalized tonic–clonic seizures

Thomas H. Rhodes[1], Carlos G. Vanoye[1], Iori Ohmori[1], Ikuo Ogiwara[2], Kazuhiro Yamakawa[2] and Alfred L. George Jr[1,3]

[1]*Division of Genetic Medicine, Department of Medicine and* [3]*Department of Pharmacology, Vanderbilt University, Nashville, TN, USA*
[2]*Laboratory for Neurogenetics, RIKEN Brain Science Institute, 2-1 Hirosawa, Wako City, Saitama 351-198, Japan*

Mutations in *SCN1A*, the gene encoding the brain voltage-gated sodium channel α_1 subunit ($Na_V1.1$), are associated with genetic forms of epilepsy, including generalized epilepsy with febrile seizures plus (GEFS+ type 2), severe myoclonic epilepsy of infancy (SMEI) and related conditions. Several missense *SCN1A* mutations have been identified in probands affected by the syndrome of intractable childhood epilepsy with generalized tonic–clonic seizures (ICEGTC), which bears similarity to SMEI. To test whether ICEGTC arises from molecular mechanisms similar to those involved in SMEI, we characterized eight ICEGTC missense mutations by whole-cell patch clamp recording of recombinant human SCN1A heterologously expressed in cultured mammalian cells. Two mutations (G979R and T1709I) were non-functional. The remaining alleles (T808S, V983A, N1011I, V1611F, P1632S and F1808L) exhibited measurable sodium current, but had heterogeneous biophysical phenotypes. Mutant channels exhibited lower (V983A, N1011I and F1808L), greater (T808S) or similar (V1611F and P1632S) peak sodium current densities compared with wild-type (WT) SCN1A. Three mutations (V1611F, P1632S and F1808L) displayed hyperpolarized conductance–voltage relationships, while V983A exhibited a strong depolarizing shift in the voltage dependence of activation. All mutants except T808S had hyperpolarized shifts in the voltage dependence of steady-state channel availability. Three mutants (V1611F, P1632S and F1808L) exhibited persistent sodium current ranging from ∼1–3% of peak current amplitude that was significantly greater than WT-SCN1A. Several mutants had impaired slow inactivation, with V983A showing the most prominent effect. Finally, all of the functional alleles exhibited reduced use-dependent channel inhibition. In summary, *SCN1A* mutations associated with ICEGTC result in a wide spectrum of biophysical defects, including mild-to-moderate gating impairments, shifted voltage dependence and reduced use dependence. The constellation of biophysical abnormalities for some mutants is distinct from those previously observed for GEFS+ and SMEI, suggesting possible, but complex, genotype–phenotype correlations.

(Received 7 July 2005; accepted after revision 5 October 2005; first published online 6 October 2005)
Corresponding author A. L. George: Division of Genetic Medicine, 529 Light Hall, Vanderbilt University, 2215 Garland Avenue, Nashville, TN 37232-0275, USA. Email: al.george@vanderbilt.edu

Neuronal voltage-gated sodium channels are responsible for the generation and propagation of action potentials in the brain and peripheral nervous system. Mutations in genes encoding sodium channel α and β_1 subunits are associated with various genetic epilepsies, including at least four distinguishable clinical syndromes with overlapping features (Wallace *et al.* 1998; Escayg *et al.* 2000; Claes *et al.* 2001; Sugawara *et al.* 2001*a*,*b*; Heron *et al.* 2002; Fujiwara *et al.* 2003; Kamiya *et al.* 2004). Several mutations identified in *SCN1A*, the gene encoding the neuronal sodium channel α_1 subunit ($Na_V1.1$), have been linked with a spectrum of disorders ranging in severity from a generally benign condition called generalized epilepsy with febrile seizures plus (GEFS+ type 2, henceforth referred to as GEFS+) to a syndrome with more devastating neurological sequelae, severe myoclonic epilepsy of infancy (SMEI). Investigation of the molecular and biophysical mechanisms underlying these disorders is expected to provide insight into the pathogenesis of epilepsy and may foster the development of new treatment methods.

The diagnosis of SMEI is based upon several clinical features including: (1) appearance of seizures,

 DOI: 10.1113/jphysiol.2005.094326

typically generalized tonic–clonic, during the first year of life; (2) impaired psychomotor development following onset of seizures; (3) occurrence of myoclonic seizures; (4) ataxia; and (5) poor response to anti-epileptic drugs (Dravet *et al.* 1992; Scheffer *et al.* 2001). Two designations, borderline SMEI (SMEB) and intractable childhood epilepsy with frequent generalized tonic–clonic seizures (ICEGTC), have been assigned to patients with an epilepsy syndrome resembling SMEI but in whom myoclonic seizures are absent and less severe psychomotor impairment is evident. Missense mutations in *SCN1A* have been reported for several patients diagnosed with either ICEGTC (Fujiwara *et al.* 2003) or SMEB (Fukuma *et al.* 2004). In contrast to SMEI, there is a notable absence of nonsense and frameshift mutations associated with these disorders. These observations indicate that SMEI, SMEB and ICEGTC are genetically related disorders exhibiting slight phenotypic differences. However, the functional perturbations of mutant SCN1A sodium channels leading to the phenotypic differences are not known.

To test the hypothesis that ICEGTC arises from molecular mechanisms similar to those causing SMEI, we studied the biophysical properties of proteins resulting from eight *SCN1A* mutations previously reported in Japanese ICEGTC kindreds. Six of the eight alleles produced functional channels with a constellation of functional abnormalities that overlapped previous findings with *SCN1A* mutations associated with both GEFS+ and SMEI. Our results provide additional evidence for a broad spectrum of biophysical abnormalities associated with *SCN1A*-linked epilepsy and further illustrate the complexity between genotype and clinical phenotype among these disorders.

Methods

Genotyping

Genomic DNA (500 ng) from patient no. 33 originally reported by Fujiwara *et al.* (2003) was subjected to long-range PCR using primers spanning *SCN1A* exons 14–16 (forward primer: TGTGGGAAAATAGCATAAGC; reverse primer: TTTGCTTTCTTCCAGATCCCG) to determine whether both mutations identified in this proband (T808S and N1011I) were present on the same or different alleles. Reactions were performed for 30 cycles (94°C for 30 s, 55°C for 1 min, and 72°C for 3.5 min) using 2.5 u of Blend Taq^{TM}-Plus DNA polymerase (Toyobo, Osaka, Japan). Amplicons were cloned into pGEM®-T Easy (Promega Corp., Madison, WI, USA) and multiple independent recombinants were sequenced. Results from two independent PCR experiments were concordant.

Mutagenesis and heterologous expression of human SCN1A

Full-length human SCN1A ($Na_V1.1$) cDNA was prepared and mutated as previously described (Lossin *et al.* 2002). Recombinant SCN1A was heterologously coexpressed with human accessory β_1 and β_2 subunits in human tsA201 cells as previously described (Lossin *et al.* 2003; Rhodes *et al.* 2004). Polymerase chain reaction site-directed mutagenesis was used to engineer individual alleles in the mammalian expression plasmid pCMV-SCN1A. The complete SCN1A open reading frame of each mutant construct was completely sequenced prior to use in experiments. At least two different recombinant clones of each mutation were evaluated electrophysiologically.

Electrophysiology and data analysis

Whole-cell patch clamp recording was used to functionally characterize wild-type (WT) and mutant sodium channels as previously described (Lossin *et al.* 2003; Rhodes *et al.* 2004). Experiments were performed at room temperature 24–72 h after transfection. Patch pipettes were pulled from borosilicate glass (Warner Instrument Co., Hamden, CT, USA) with a multistage P-97 Flaming-Brown micropipette puller (Sutter Instruments Co., San Rafael, CA, USA) and fire polished with a microforge MF 830 (Narashige, Japan). Pipette resistance was 1.0–1.6 MΩ. The bath solution (containing (mM): NaCl, 145; KCl, 4; $CaCl_2$, 1.8; $MgCl_2$, 1; and Hepes, 10; pH 7.35, 310 mosmol kg^{-1}) was continuously exchanged by a gravity-driven perfusion system. The pipette solution consisted of (mM): NaF, 10; CsF, 110; CsCl, 20; EGTA, 2; and Hepes, 10; pH 7.35, 310 mosmol kg^{-1}. As a reference electrode, a 2% agar bridge with composition similar to the bath solution was used. Cells were allowed to stabilize for 10 min after establishment of the whole-cell configuration before current was measured. Recordings from cells exhibiting peak current amplitudes less than 0.6 nA were excluded from analysis to avoid potential endogenous channel contamination. Cells exhibiting very large whole-cell currents were also excluded if voltage control was compromised. Whole-cell capacitance and access resistance were determined by integrating capacitive transients of voltage steps from −120 to −110 mV filtered at 5 kHz. Series resistance (2 ± 0.1 MΩ) was compensated 87–95% to assure that the command potential was reached within microseconds and with a voltage error < 3 mV. Leak current was subtracted using a $P/4$ procedure. All data were acquired at 10–50 kHz and lowpass filtered at 5 kHz. Specific voltage-clamp protocols assessing channel activation, fast inactivation and slow inactivation are depicted in each figure. Persistent current was evaluated by 200 ms depolarizations to −10 mV. The level of tetrodotoxin (TTX)-sensitive persistent current

was determined at the end of the 200 ms depolarization and expressed as a percentage of peak current following digital subtraction of currents recorded in the presence and absence of 10 μM TTX (Sigma, St Louis, MO, USA).

To describe fast inactivation quantitatively, the decay phase of voltage-sensitive inward currents was fitted with a two-exponential function,

$$I/I_{\max} = A_1 \exp(-t/\tau_1) + A_2 \exp(-t/\tau_2) + C,$$

where A and τ refer to fractional amplitudes and time constants, respectively, while C represents a non-inactivating current component. Conductance–voltage and steady-state availability curves were fitted with Boltzmann functions to determine the voltages for half-maximal activation and inactivation ($V_{1/2}$) and slope factor (k). Recovery from fast inactivation was analysed by fitting data to a two-exponential function,

$$I/I_{\max} = A_1[1 - \exp(-t/\tau_1)] + A_2[1 - \exp(-t/\tau_2)],$$

where A and τ are fractional amplitudes and time constants, respectively. Analyses of slow inactivation data were performed as previously described (Lossin *et al.* 2003; Rhodes *et al.* 2004). Data analyses were performed using Clampfit (Axon Instruments, Union City, CA, USA), Excel (Microsoft, Seattle, WA, USA) and OriginPro (OriginLab Corporation, Northampton, MA, USA) software as previously described (Lossin *et al.* 2003; Rhodes *et al.* 2004). All data were fitted using a non-linear least-squares minimization method. Results are presented as means ± S.E.M., and statistical comparisons were made between data from mutant and WT sodium channels using Student's unpaired t test. Statistical significance was assumed for $P < 0.05$. In some figures, the standard error bars are smaller than the data symbols.

Results

We examined the biophysical properties of eight missense ICEGTC mutants (Fig. 1) using whole-cell patch clamp recording of heterologously expressed recombinant human SCN1A sodium channels coexpressed with human β_1 and β_2 subunits. All mutations were originally identified in Japanese ICEGTC probands and were reported by Fujiwara *et al.* (2003). In one individual reported in this study (patient no. 33), two *de novo* mutations were discovered (T808S and N1011I), while all other subjects were heterozygous for single alleles. To determine whether T808S and N1011I occurred on the same or different *SCN1A* alleles, we sequenced long-range PCR-generated amplicons derived from genomic DNA of this individual. The two mutations were not found in the same PCR products and thus are demonstrated to reside on separate alleles.

Biophysical properties of ICEGTC mutants

Six of the eight mutations exhibited functional sodium channel activity when transiently expressed in tsA201 cells. The two non-functional alleles, G979R and T1709I, affect residues located within the D2/S6 segment and D4 pore loop, respectively (Fig. 1). We ruled out cloning artifacts as an explanation for non-functional sodium channels by verifying the complete coding sequence of each mutant construct and by examining multiple independent recombinant clones. Interestingly, the rat orthologue of human *SCN1A* (GenBank accession NP_110502) has an arginine residue in the position corresponding to the G979R mutation.

Figure 2 illustrates representative whole-cell currents evoked by a series of depolarizing test potentials in cells expressing either WT-SCN1A or each one of the six mutant channels. There was considerable variation in the amplitude of expressed sodium currents observed in these experiments. Current–voltage relationships (Fig. 3*A*) illustrate that mutant channels exhibited lower (V983A, $P < 0.05$; N1011I, $P < 0.05$; and F1808L, $P < 0.005$), greater (T808S, $P < 0.005$), or similar (V1611F, P1632S) peak sodium current densities at −10 mV compared with WT-SCN1A. Current densities exhibited by cells expressing P1632S were significantly greater than WT-SCN1A only at voltages between −50 and −20 mV ($P < 0.005$).

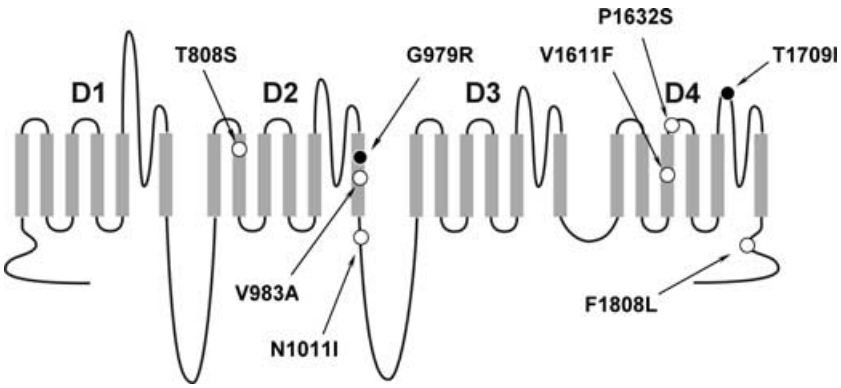

Figure 1. Location of SCN1A mutations
Schematic diagram illustrating the transmembrane topology of a voltage-gated sodium channel and location of ICEGTC mutations characterized in this study. Filled symbols represent non-functional mutations and open symbols represent the location of mutations with preserved activity.

Disturbances in activation and inactivation

Qualitative differences in the time course of whole-cell current decay (see superimposed normalized traces in bottom right panel of Fig. 2) and shifts in peak current density along the voltage axis (Fig. 3*A*) were evident for many of the mutants. These observations prompted more detailed analyses of activation and inactivation properties. In some mutants, the voltage dependence of channel activation was significantly shifted in either the depolarized (V983A) or hyperpolarized direction (P1632S, V1611F and F1808L; Fig. 3*B* and Table 1). Depolarizing shifts in conductance–voltage curves have been previously reported for SCN1A mutants associated with GEFS+ and SMEI (Lossin *et al.* 2003; Rhodes *et al.* 2004). Hyperpolarizing shifts in activation have been previously observed only for the GEFS+ mutant W1204R expressed in *Xenopus* oocytes using the rat *SCN1A* orthologue (Spampanato *et al.* 2003), but not when it was expressed in cultured human cells using human SCN1A (Lossin *et al.* 2002).

The voltage dependence of channel availability following 100 ms depolarizations to a range of potentials was shifted in the hyperpolarizing direction by 7–22 mV for all mutants except T808S, which was not different from WT-SCN1A (Fig. 3*C* and Table 1). For two alleles (P1632S and F1808L), the magnitude of voltage shift in channel availability was greater than the shift in the corresponding activation curve. Similarly, V983A exhibited opposing shifts in activation (+6 mV) and channel availability (−17 mV), suggesting that reduced channel function may be the net consequence. Figure 4 illustrates these two distinct patterns of altered voltage dependence represented by P1632S (hyperpolarized activation and inactivation) and V983A (depolarized activation, but hyperpolarized inactivation). These data revealed that the window current, as defined by the area of overlap between activation and inactivation curves, appeared smaller in the mutants than in WT-SCN1A.

Recovery from fast inactivation was evaluated using a two-pulse protocol illustrated in Fig. 3*D*, and the data were

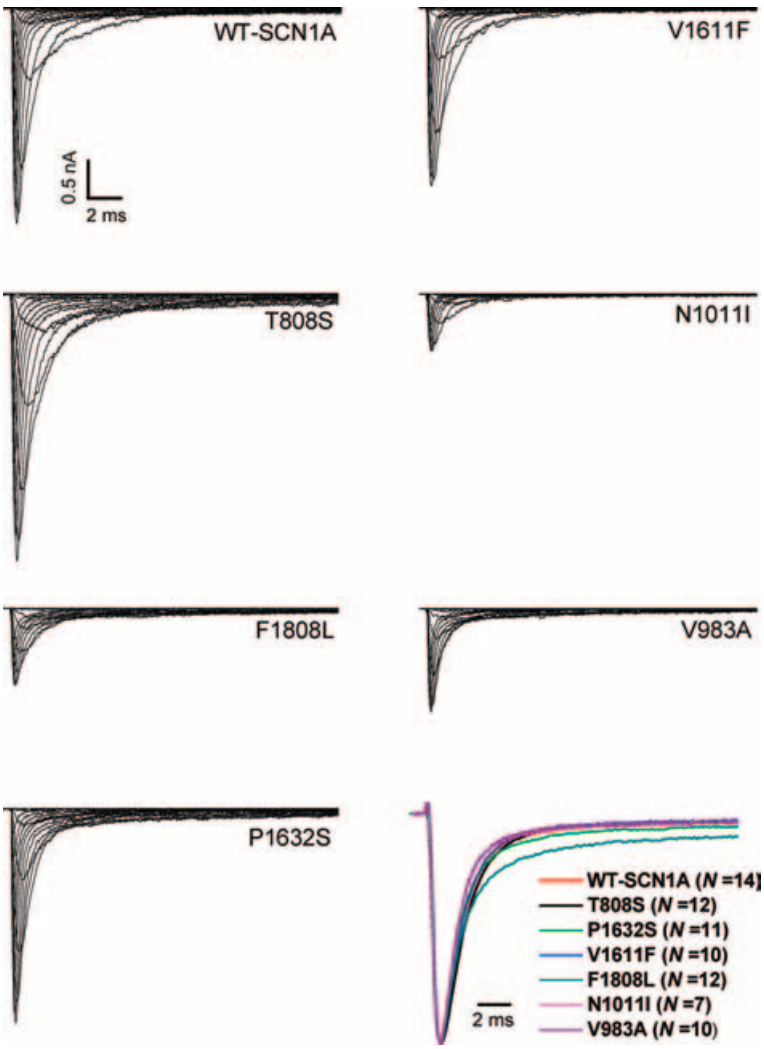

Figure 2. Representative WT and mutant whole-cell SCN1A sodium currents
Whole-cell currents recorded from tsA201 cells transiently expressing the indicated alleles during voltage steps to various potentials between −80 and +60 mV in 10 mV intervals from a holding potential of −120 mV (see pulse protocol illustrated in Fig. 3*B*). Vertical and horizontal scale bars represent 0.5 nA and 2 ms, respectively. The lower right panel illustrates superimposed averaged whole-cell sodium currents evoked by depolarization to 0 mV from a holding potential of −120 mV and normalized to peak current amplitude. Values in parentheses indicate the number of independent cells used to obtain each averaged current trace.

fitted with a two-exponential function as described in the Methods. Recovery proceeded with a bi-exponential time course, with the major fraction of channels recovering within a few milliseconds (described by time constant, τ_1, Table 1) and a minor population recovering more slowly (τ_2). In cells expressing T808S, N1011I or V983A, recovery from inactivation was slower, as evidenced by the larger time constant representing the faster component (τ_1, Table 1). Similarly, two mutants, V1611F and F1808L, exhibited a significantly larger proportion of channels recovering with the slower component (Table 1). None of the ICEGTC mutants we studied had faster recovery from inactivation.

The kinetics of fast inactivation were characterized in more detail by fitting the decay phase of sodium current traces with a two-exponential function as described in the Methods. Figure 5 illustrates differences among mutants in their time constants (Fig. 5*A*) and slow component amplitude (Fig. 5*B*). Overall, there were relatively minor differences in the time constants of inactivation among the six mutants compared with WT-SCN1A. For three mutations (P1632S, F1808L and V1611F) the fast time constant for inactivation (τ_1) was significantly smaller at the most negative test potentials, while in one allele (V983A) we observed a smaller τ_1 only at positive voltages (*P* values given in Fig. 5 legend). There were no significant

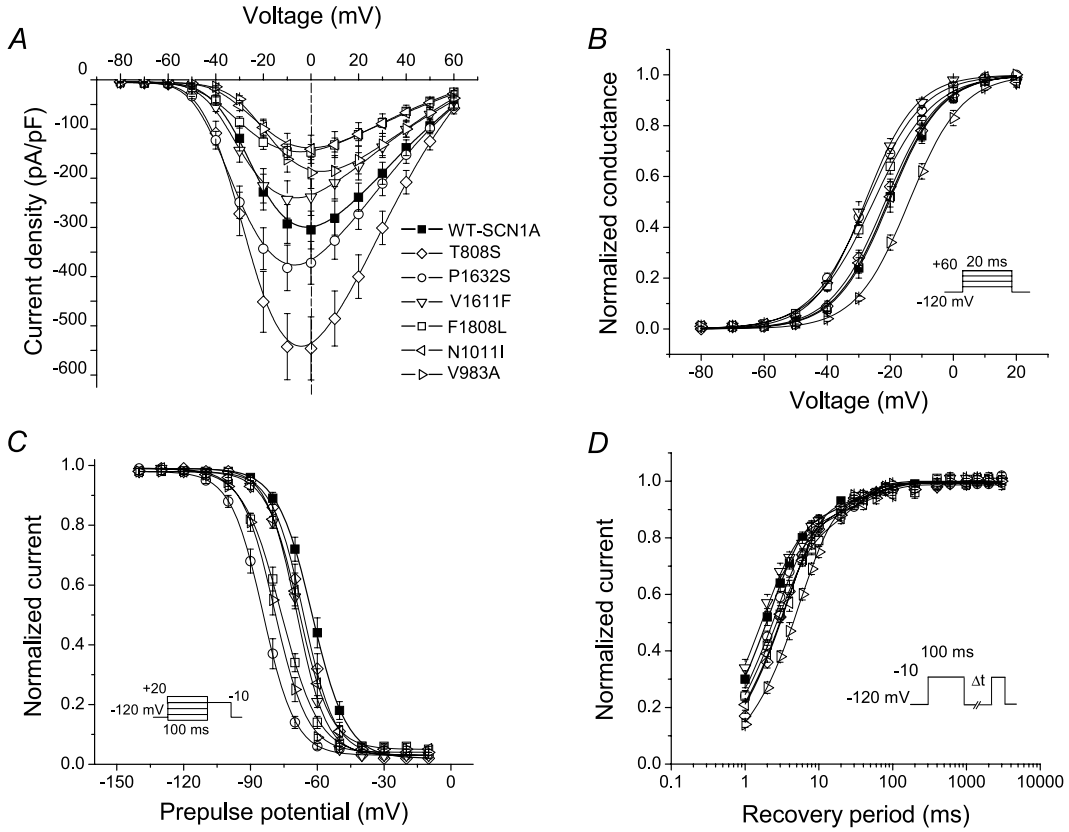

Figure 3. Inactivation and activation properties of ICEGTC-associated mutants
A, current–voltage relationships of whole-cell currents from transiently transfected tsA201 cells. Currents were elicited by test pulses to various potentials (*B*, inset) and normalized to cell capacitance (WT-SCN1A, $n = 14$; T808S, $n = 12$; P1632S, $n = 10$; V1611F, $n = 12$; F1808L, $n = 11$; N1011I, $n = 6$; V983A, $n = 9$). T808S current density is significantly larger than WT between −50 and +60 mV ($P < 0.05$). P1632S current density is significantly larger than WT between −40 and −20 mV ($P < 0.05$). F1808L and N1011I current density is significantly smaller than WT between −20 and +60 mV ($P < 0.05$). V983A current density is significantly smaller than WT between −30 and 0 mV ($P < 0.05$). *B*, voltage dependence of activation. The voltage dependence of channel activation was estimated by measuring peak sodium current during a variable test potential step from a holding potential of −120 mV. The current at each membrane potential was divided by the electrochemical driving force for sodium ions and normalized to the maximum sodium conductance. *C*, voltage dependence of inactivation. The two-pulse protocol outlined in the inset was used to examine channel availability after conditioning at various potentials. Currents were normalized to the peak current amplitude. *D*, recovery from fast inactivation. Channels were inactivated by a 100 ms pulse and then stepped to −120 mV for increasingly long periods. Currents were normalized to the peak current amplitude measured during the inactivation pulse and fitted to a two-exponential function generating fast and slow recovery time constants. Fitted values from these experiments are provided in Table 1.

Table 1. Biophysical parameters for activation and fast inactivation

	Voltage dependence of activation			Voltage dependence of fast inactivation			Recovery from fast inactivation		
	$V_{½}$ (mV)	k (mV)	n	$V_{½}$ (mV)	k (mV)	n	τ_1 (ms)¶	τ_2 (ms)¶	n
WT-SCN1A	−19.4 ± 1.4	7.9 ± 0.2	13	−62.7 ± 1.7	−6.9 ± 0.2	14	2.4 ± 0.3 [85 ± 1%]	41 ± 6 [15 ± 1%]	14
P1632S	−27.3 ± 1.0‡	8.7 ± 0.2*	10	−84.7 ± 1.5§	−7.1 ± 0.3	9	2.7 ± 0.2 [82 ± 1%]	45 ± 5 [18 ± 1%]	8
V1611F	−27.9 ± 1.2‡	7.5 ± 0.2	11	−69.5 ± 0.9*	−6.8 ± 0.2	11	1.8 ± 0.2 [80 ± 2%*]	32 ± 5 [20 ± 1%*]	10
F1808L	−25.3 ± 1.3*	9.2 ± 0.2‡	12	−77.1 ± 1.3§	−7.9 ± 0.2†	11	2.5 ± 0.2 [69 ± 4%‡]	32 ± 5 [31 ± 4%‡]	11
T808S	−21.7 ± 1.3	8.3 ± 0.2	11	−66.5 ± 1.6	−6.9 ± 0.3	10	3.8 ± 0.3† [89 ± 1%]	63 ± 7* [11 ± 1%]	9
N1011I	−20.5 ± 1.9	8.1 ± 0.2	6	−70.1 ± 0.4*	−7.3 ± 0.4	6	3.4 ± 0.3* [85 ± 2%]	58 ± 6 [14 ± 3%]	6
V983A	−13.9 ± 1.1*	8.2 ± 0.3	8	−79.3 ± 1.5§	−7.1 ± 0.2	9	5.4 ± 0.5§ [83 ± 3%]	37 ± 4 [16 ± 3%]	8

Values statistically significantly different from WT-SCN1A are indicated as follows: *$P < 0.05$; †$P < 0.005$; ‡$P < 0.0005$; §$P < 0.0001$. ¶ values in square brackets are amplitude

differences between WT-SCN1A and mutant channels with regard to the slow time constant (τ_2), except for V1611F at +30 mV. However, three alleles did exhibit differences in the distribution of inactivation into fast and slow components (Fig. 5*B*), with larger slow component fractional amplitudes observed for F1808L in the −20 to +30 mV range. The impact of F1808L on the slow component amplitude helped to explain the delayed time course of inactivation observed in Fig. 2. Similarly, P1632S and V983A exhibited significantly larger slow component fractional amplitudes at 0 and +10 mV.

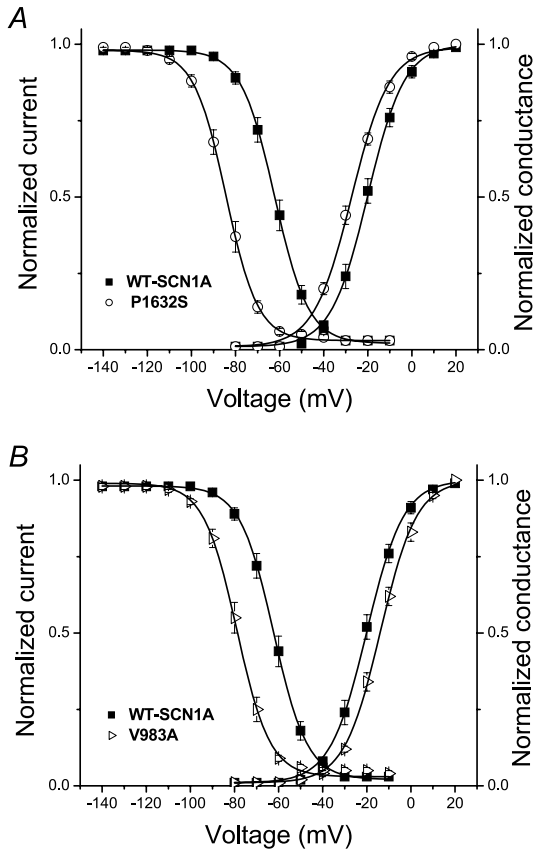

Figure 4. Altered voltage dependence of activation and inactivation

A, plots of steady-state inactivation and conduction–voltage curves for WT-SCN1A (■) and P1632S (○). *B*, similar plots for WT-SCN1A (■) and V983A (▷). Data are the same as shown in Fig. 3*B* and *C*, with fit parameters given in Table 1.

ICEGTC mutants exhibit persistent sodium current

Previously, we have demonstrated that a subset of *SCN1A* mutations associated with GEFS+ and SMEI exhibited persistent, non-inactivating sodium current (I_{Na}), and this phenomenon may be an important biophysical feature of mutant sodium channels associated with inherited epilepsy (Lossin *et al.* 2002; Rhodes *et al.* 2004). We examined the six functional ICEGTC alleles for persistent I_{Na}, and the results of these experiments are illustrated in Fig. 6. Cells expressing three mutations (P1632S, V1611F and F1808L) exhibited significantly greater levels of persistent I_{Na} compared to WT-SCN1A. For P1632S and V1611F the level of persistent I_{Na} was ∼1% of peak current, whereas F1808L exhibited persistent I_{Na} of more than 3% peak current. All three of these mutations affect residues in the D4 domain (S3 segment or S3–S4 linker) or the adjacent region of the carboxyl tail (F1808L). The F1808L mutation is located within a highly conserved acidic domain that exists in voltage-gated sodium channels and resembles an EF-hand motif (Babitch & Anthony, 1987). The corresponding region in cardiac sodium channels has been shown to bind calcium ions and is affected by mutations associated with inherited arrhythmias (Wingo *et al.* 2004). Additional experimental work has defined the sodium channel C-terminus as an important domain for fast inactivation (Motoike *et al.* 2004).

Alterations in slow inactivation

Sodium channels have distinct mechanisms for modulating their activity over a longer time course than fast inactivation. In mutant channels, defects in slow inactivation may be significant in determining the steady-state level of channel availability. We tested the six functional ICEGTC alleles for differences in slow inactivation properties, and results from these experiments are illustrated in Fig. 7, with quantitative parameters provided in Table 2. The onset of slow

inactivation proceeded with a bi-exponential time course for WT-SCN1A and all mutant channels (Fig. 7*A*). All mutations except F1808L exhibited significant differences in time constants or fractional amplitudes for slow inactivation. The greatest differences were observed for V983A, which has a much larger time constant describing the slower component of onset (Table 2). V983A also exhibits a significantly altered voltage dependence of slow inactivation (Fig. 7*B*), with a large shift in $V_{1/2}$ to more positive potentials, and more rapid recovery (Fig. 7*C* and Table 2). Other mutant alleles also exhibit impaired onset of slow inactivation (P1632S, T808S and N1011I), but in combination with slower recovery. These observations informed us that slow inactivation is disrupted to varying degrees in the ICEGTC mutants.

ICEGTC mutants have reduced use-dependent inhibition

During rapid stimulation, voltage-gated sodium channels may exhibit use dependence when the time between successive depolarizations is less than the time required for complete recovery from inactivation. We examined use-dependent channel inhibition by stimulating cells expressing WT-SCN1A or mutants with depolarizing pulse trains at varying frequencies (Fig. 8*A*). Despite the heterogeneity of biophysical disturbances displayed by the ICEGTC mutants, all alleles exhibited a trend toward reduced use dependence, with V983A, V1611F and F1808L having significant differences at the highest stimulation frequencies. At a pulsing frequency of 60 Hz, the residual current in cells expressing each of the mutant alleles was significantly greater than in cells expressing WT-SCN1A (Fig. 8*B*). Reduced use dependence may support enhanced firing of neurones expressing the mutant channels and thus contribute to the pathogenesis of ICEGTC.

Discussion

Germ line mutations in neuronal voltage-gated sodium channel genes have been associated with at least four identifiable clinical epilepsy syndromes. The majority of

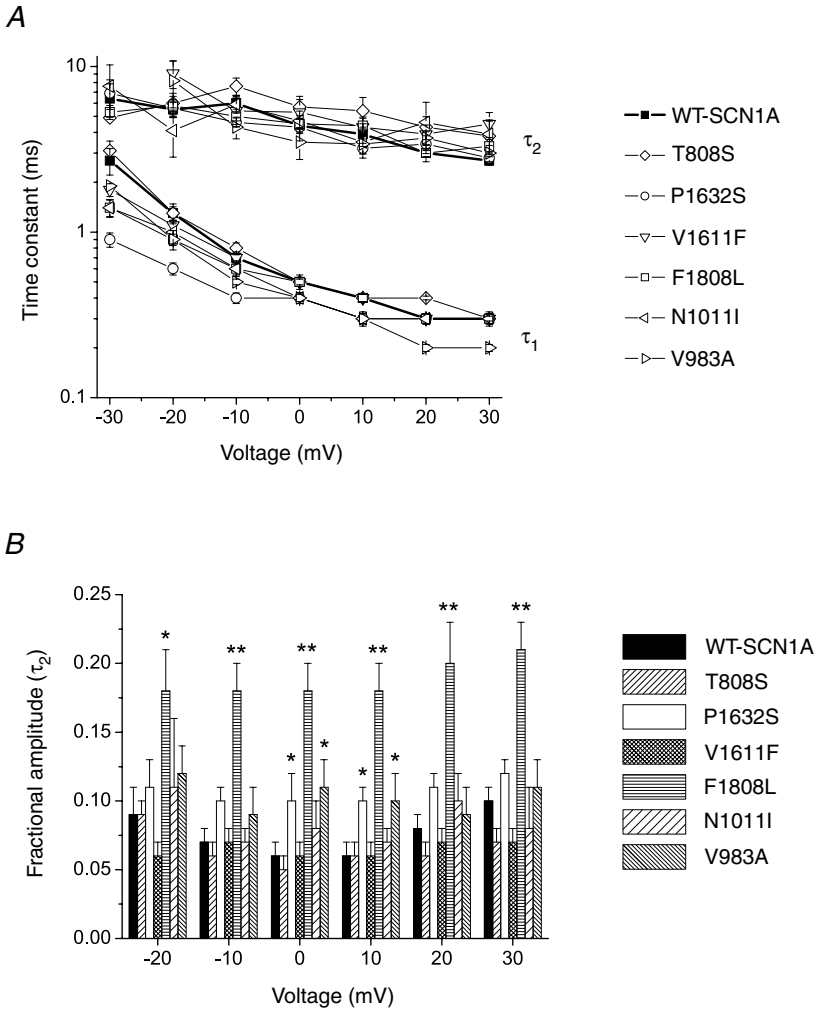

Figure 5. Voltage dependence of fast inactivation time constants and fractional amplitudes
A, inactivation time constants for WT and mutant SCN1A currents plotted against test voltage. The decay phase of the transient sodium current was fitted with a two-exponential function as described in the Methods. Fast time constants (τ_1) were significantly smaller for P1632S (−10 to −30 mV, $P < 0.005$; and 0 mV, $P < 0.05$), V983A (−10 and +30 mV, $P < 0.05$), F1808L (−30 mV, $P < 0.05$), and V1611F (−30 mV, $P < 0.05$). Significantly larger τ_1 values were observed for T808S (+20 mV, $P < 0.05$) and V1611F (+30 mV, $P < 0.05$). *B*, fractional amplitudes of the slower component (τ_2) of fast inactivation plotted against voltage (values significantly different from WT are indicated as $^*P < 0.05$ and $^{**}P < 0.005$).

reported mutations occur in *SCN1A*, for which more than 100 alleles have been described (Escayg *et al.* 2000, 2001; Abou-Khalil *et al.* 2001; Claes *et al.* 2001; Claes *et al.* 2003; Ito *et al.* 2002; Ohmori *et al.* 2002; Wallace *et al.* 2001; Sugawara *et al.* 2001*a*, 2002; Heron *et al.* 2002; Fujiwara *et al.* 2003; Kamiya *et al.* 2004). This level of allelic heterogeneity exceeds that observed for inherited muscular and cardiac disorders caused by mutation of *SCN4A* and *SCN5A*, respectively. Establishment of genotype–phenotype correlations and elucidation of the molecular basis for brain sodium channelopathies are important goals that may shed light on epileptogenesis.

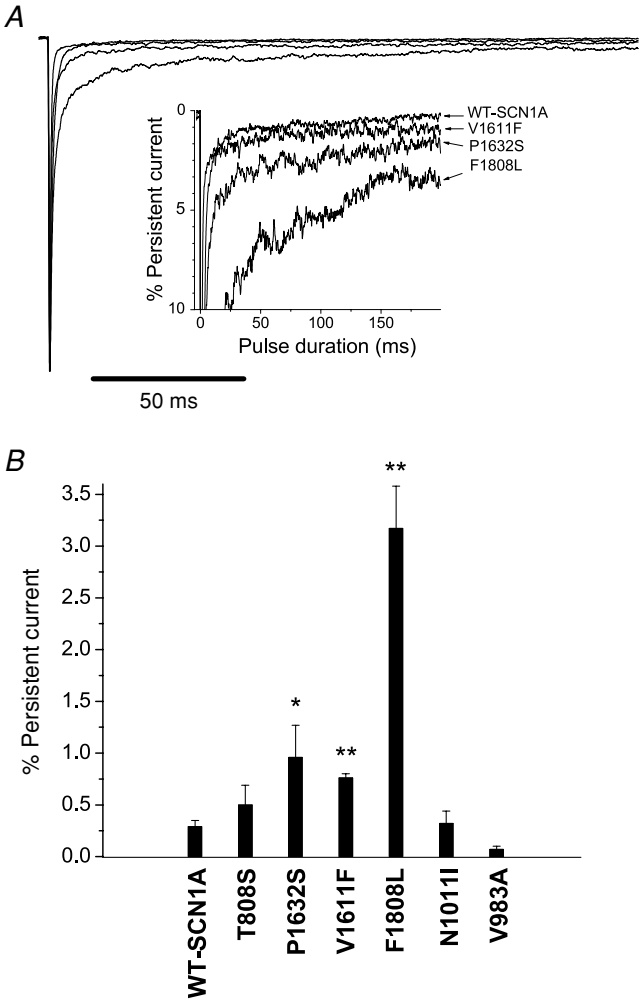

Figure 6. ICEGTC mutants exhibit persistent sodium current
A, sodium current was measured at the end of a 200 ms depolarization to −10 mV from a holding potential of −120 mV. TTX-sensitive currents were obtained by digital subtraction of sodium currents recorded before and after TTX addition. Sodium currents were normalized to peak amplitude. The inset shows an expanded vertical scaled to emphasize the relative proportion of persistent current. *B*, persistent sodium current expressed as the percentage of peak current amplitude for WT-SCN1A ($n = 9$) and the six ICEGTC mutants ($n = 4$–6). Values significantly different from WT are indicated as $^{*}P < 0.05$ and $^{**}P < 0.005$.

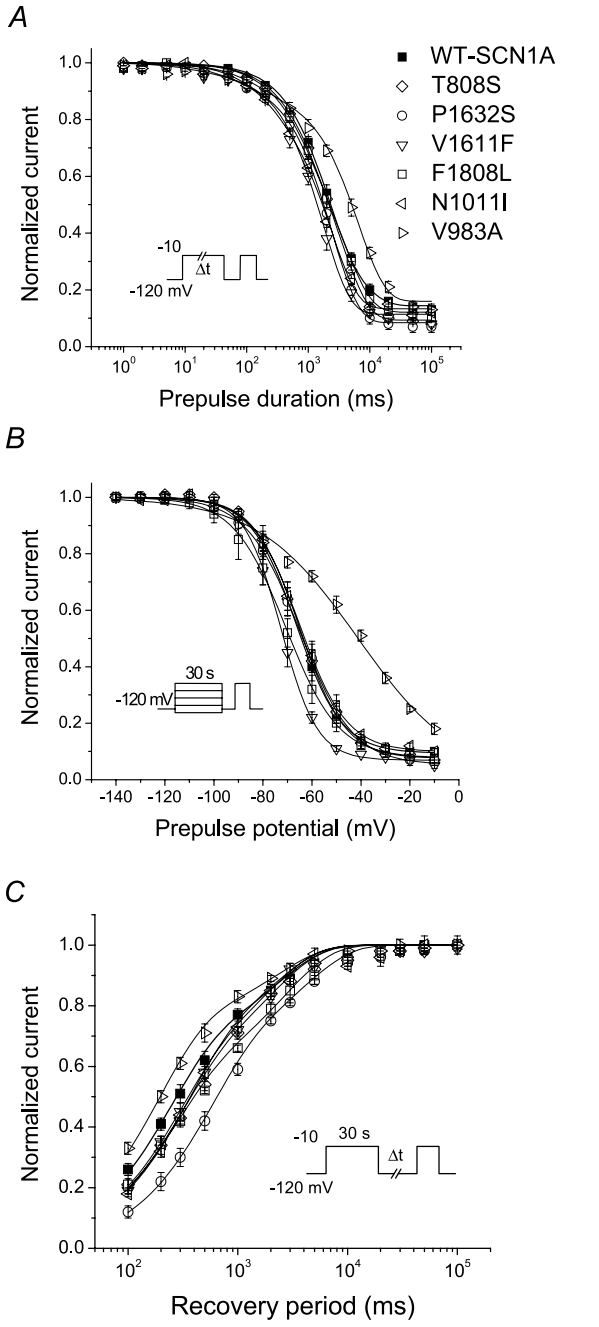

Figure 7. Slow inactivation properties of WT and mutant SCN1A channels
A, onset of slow inactivation. Cells were stepped to −10 mV for 0.001–100 s, allowed to recover from fast inactivation at −120 mV for 50 ms, and subjected to a −10 mV test pulse. *B*, steady-state slow inactivation after a 30 s depolarization to potentials between −140 and −10 mV. Cells were allowed to recover from fast inactivation at −120 mV for 50 ms before a test pulse to −10 mV. *C*, recovery from slow inactivation. Cells were conditioned at −10 mV for 30 s, allowed to recover at −120 mV for 0.1–100 s, and immediately tested at −10 mV. Because the recovery period always exceeded 100 ms, effects of fast inactivation were considered negligible. Data were fitted to a two-exponential (*A* and *C*) or a Boltzmann function (*B*), as described in the Methods. Fitted values from all experiments are provided in Table 2.

Table 2. Biophysical parameters for slow inactivation

	Onset of slow inactivation				Voltage dependence of slow inactivation				Recovery from slow inactivation		
	τ_1 (ms)	τ_2 (ms)	Mean I_r§	n	$V_{½}$ (mV)	k (mV)	Mean I_r§	n	τ_1 (ms)§	τ_2 (ms)§	n
WT-SCN1A	30 ± 7	3029 ± 283	14 ± 1	14	−66.7 ± 2.0	7.8 ± 0.2	10 ± 1	11	238 ± 16	2487 ± 240	11
	(3 ± 1%)	(83 ± 1%)							[65 ± 3%]	[35 ± 3%]	
P1632S	60 ± 13*	2576 ± 113	7 ± 2†	6	−64.8 ± 2.2	10.4 ± 1.0‡	5 ± 1*	6	607 ± 72‡	5210 ± 615‡	7
	(6 ± 1%‡)	(86 ± 2%)							[67 ± 2%]	[33 ± 2%]	
V1611F	28 ± 12	1873 ± 269*	11 ± 1	5	−72.8 ± 1.7	7.1 ± 0.3	7 ± 2*	6	291 ± 17	2765 ± 306	6
	(4 ± 1%)	(86 ± 1%)							[63 ± 3%]	[37 ± 3%]	
F1808L	32 ± 6	3013 ± 382	12 ± 1	7	−71.0 ± 2.0	10.9 ± 1.4‡	7 ± 2	4	269 ± 13	3362 ± 461	5
	(4 ± 1%)	(84 ± 1%)							[57 ± 1%]	[43 ± 1%*]	
T808S	71 ± 12‡	3099 ± 370	9 ± 1†	8	−65.0 ± 1.7	9.2 ± 0.5*	7 ± 1	6	340 ± 57*	3412 ± 685	6
	(4 ± 1%)	(87 ± 1%*)							[65 ± 5%]	[35 ± 5%]	
N1011I	77 ± 18*	2283 ± 172	12 ± 2	5	−65.0 ± 2.5	9.3 ± 0.5*	10 ± 1	5	338 ± 27‡	4369 ± 1388	5
	(8 ± 1%‡)	(80 ± 2%)							[67 ± 8%]	[31 ± 8%]	
V983A	60 ± 13*	6549 ± 606‡	15 ± 2	7	−42.5 ± 2.5**	19.4 ± 0.3‡	3 ± 3*	5	169 ± 7*	2271 ± 566	5
	(9 ± 1%‡)	(76 ± 1%‡)							[68 ± 5%]	[31 ± 5%]	

I_r, residual current. Values statistically significantly different from WT are indicated as follows: *$P < 0.05$; †$P < 0.01$; ‡$P < 0.005$. § values in square brackets are amplitude

In this study, we characterized the detailed biophysical properties of several missense *SCN1A* mutations identified in patients with ICEGTC, a disorder closely related to SMEI. Our primary goal was to determine whether there were specific patterns of sodium channel dysfunction that resemble the biophysical defects observed for SMEI-associated mutations. However, our findings indicate that a diversity of biophysical phenotypes exist, which show overlap with missense alleles associated with GEFS+ and SMEI. The spectrum of functional defects exhibited by ICEGTC mutations further indicates the complexity of molecular mechanisms that operate in these disorders.

Diversity of biophysical phenotypes in ICEGTC

The *SCN1A* mutations we studied exhibited a range of defects in the voltage dependence and kinetics of activation, fast inactivation and slow inactivation. Abnormal voltage dependence of activation with

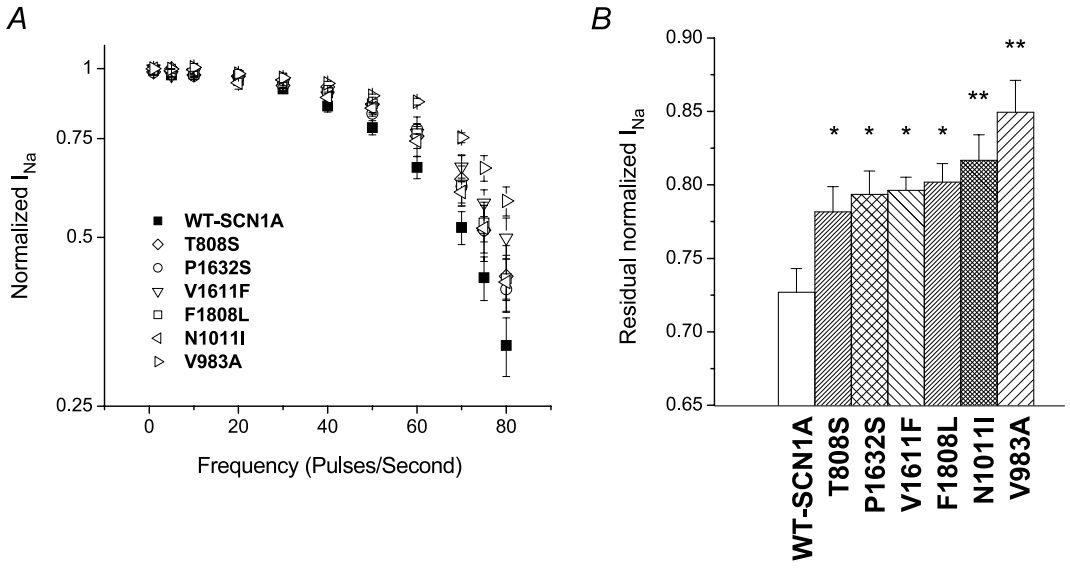

Figure 8. Use dependence of WT and mutant SCN1A channels
A, frequency dependence of WT-SCN1A and ICEGTC mutants. Cells were stimulated with depolarizing pulse trains (100 pulses, 5 ms, 0 mV) from a holding potential of −120 mV at the indicated frequencies. A recovery interval (15 s, −120 mV) followed each pulse train experiment. Currents were normalized to the value recorded after the first pulse in each frequency train for the corresponding allele and plotted on a log scale. Data are means ± S.E.M. from 3 or 4 cells. Significant differences ($P < 0.05$) from WT-SCN1A were observed for V983A (40–80 Hz), V1611F (60–80 Hz) and F1808L (50–80 Hz). *B*, residual normalized sodium current after the 60th pulse during a 60 Hz pulse train ($n =$ 5–7 cells). Significant differences from WT-SCN1A are indicated as *$P < 0.05$ and **$P < 0.005$.

Table 3. Predicted influence of biophysical properties on net channel activity

Biophysical property	P1632S	F1808L	V1611F	T808S	N1011I	V983A
Peak current density	↑	↓	—	↑	↓	↓
Activation $V_{1/2}$	↑	↑	↑	—	—	↓
Persistent I_{Na}	↑	↑	↑	—	—	—
Inactivation $V_{1/2}$	↓	↓	↓	—	↓	↓
Recovery from inactivation	—	↓	↓	↓	↓	↓
Slow inactivation	↓/↑	—/↓	—/↓	↓/↑	↓/↑	↑

↑, predicted gain of channel activity;↓, predicted loss of channel activity; —, no predicted change in channel activity; ↓/↑, uncertain or mixed effects.

either hyperpolarizing (P1632S, V1611F and F1808L) or depolarizing shifts (V983A) was observed in cells expressing four of the studied alleles. All ICEGTC mutations we studied, except T808S, caused hyperpolarizing shifts in the voltage dependence of steady-state inactivation. Considering both activation and inactivation, we observed three patterns of altered voltage dependence among these mutations. One group of alleles (P1632S, V1611F and F1808L) caused hyperpolarizing shifts in both activation and inactivation. For P1632S and F1808L, the shift in voltage dependence of inactivation was greater than the corresponding shift in activation, indicating that there is less overlap in these relationships (i.e. reduced window current) than for WT-SCN1A. By contrast, V983A caused shifts in opposite directions for activation (depolarizing) and inactivation (hyperpolarizing) voltage dependence (Fig. 4). Finally, N1011I exhibited a hyperpolarizing shift in inactivation but no difference in the voltage dependence of activation. Overall, these patterns of altered voltage dependence suggest reduced channel availability, which could be indirectly related to enhanced neuronal excitability through a mechanism involving suppression of inhibitory neuronal networks. None of the mutations we studied exhibited a depolarizing shift in voltage dependence of inactivation, which has been implicated as a major contributor to neuronal hyperexcitability for one *SCN1A* allele (D1866Y) linked to GEFS+ (Spampanato *et al.* 2004).

Abnormalities in the kinetics of fast inactivation were prominent for P1632S and F1808L, with more subtle but significant changes observed for V1611F and V983A. Three of these mutants exhibited persistent I_{Na} (V1611F, P1632S and F1808L), ranging between 1 and 3% of the peak current. This phenomenon has been observed for missense mutations associated with both GEFS+ and SMEI and is therefore not phenotype specific. Mechanistically, the increased persistent I_{Na} observed for these mutations cannot be explained by an increased window current. Increased persistent I_{Na} has great potential for disrupting neuronal excitability and has previously been observed as a common gating disturbance associated with mutations in *SCN4A* and *SCN5A* linked to hyperkalaemic periodic paralysis (Cannon & Strittmatter, 1993) and the congenital long QT syndrome (Bennett *et al.* 1995), respectively.

We also observed significant changes in slow inactivation properties of several mutants, with the most dramatic effects caused by V983A. This mutation exhibited impaired slow inactivation characterized by a slower time course of onset and a depolarizing shift in voltage dependence. Impaired slow inactivation is predicted to increase channel availability during prolonged or repetitive membrane depolarizations. However, V983A also exhibited a faster recovery from slow inactivation, which implies a reduced stability of the slow inactivated state. Other mutations also displayed mixed changes in slow inactivation (Table 2) that do not have easily predictable effects on neuronal excitability.

Pathophysiological implications

Most *SCN1A* mutations associated with SMEI are predicted to encode non-functional channels by premature termination or frameshift of the coding sequence. This observation underlies the hypothesis that SMEI, and perhaps other epilepsy syndromes linked to neuronal sodium channel mutations, stem from *SCN1A* haploinsufficiency (Yamakawa, 2005). Consistent with this idea is the finding that some missense mutations associated with SMEI are non-functional or exhibit marked attenuation in activity (Lossin *et al.* 2003; Sugawara *et al.* 2003; Rhodes *et al.* 2004). By contrast, certain GEFS+ mutations cause persistent I_{Na} or other functional changes predicting enhanced channel availability (Spampanato *et al.* 2001). However, a simple dichotomy of 'gain' *versus* 'loss' of function to explain clinical differences between GEFS+ and SMEI is almost certainly an oversimplification, as illustrated by the demonstration of non-functional *SCN1A* alleles associated with GEFS+ and large persistent I_{Na} exhibited by certain SMEI mutations (Lossin *et al.* 2003; Rhodes *et al.* 2004). Given the clinical similarities between SMEI and ICEGTC, one could have predicted similar behaviours among the respective causative mutations. In support of this notion, Fukuma *et al.* (2004) reported that two specific missense mutations in SCN1A (M924I and R936C) were discovered

in subjects with either SMEI or borderline SMEI. To date, frameshift and nonsense mutations have not been observed in ICEGTC or borderline SMEI, but we did observe two non-functional ICEGTC alleles. However, we did not observe a close correlation between the biophysical properties of ICEGTC and SMEI mutations. In fact, the behaviour of certain ICEGTC alleles more closely resembled the defects exhibited by GEFS+ mutations. We also find it interesting that two of the ICEGTC mutations we tested (V1611F and T1709I) cause the milder epilepsy syndrome, GEFS+, in the parent from whom the mutation was inherited (Fujiwara *et al.* 2003). In each of these cases, the ICEGTC proband was male and the mutation was transmitted from the mother. These observations suggest that other host factors, such as gender and possibly modifier genes, may impact disease expression.

Our study reveals a complex relationship between the clinical syndrome and biophysical behaviours of the mutant sodium channels. Whether the net effect of these functional changes is predominantly a gain or loss of channel activity cannot easily be discerned. We summarized the predicted influence of the observed biophysical properties of each mutation on sodium channel activity (Table 3). Interestingly, despite the considerable biophysical heterogeneity, all mutations exhibited reduced use-dependent inhibition (Fig. 8), and this may be an important common factor in the pathogenesis of *SCN1A*-linked epilepsy. Attenuated use dependence has also been observed for certain *SCN1A* alleles associated with GEFS+ when examined in the *Xenopus* oocyte expression system (Spampanato *et al.* 2001, 2004), but has not been examined for mutations associated with SMEI. We can speculate that this effect will enable mutant sodium channels to facilitate high-frequency neuronal firing, but directly demonstrating changes in neuronal excitability caused by these patterns of sodium channel dysfunction will require additional studies of animal models or advanced computational simulations.

Effects of compound heterozygosity for *SCN1A* mutations

One ICEGTC proband reported by Fujiwara and colleagues carried two mutations on separate *SCN1A* alleles (T808S and N1011I), but the described phenotype in this case was no more severe than simple heterozygous carriers (Fujiwara *et al.* 2003). Our functional studies indicate that both T808S and N1011I exhibit milder biophysical phenotypes, which we presume sum to produce the clinical disorder. Another possible mechanism to reconcile the clinical similarities associated with simple and compound heterozygosity is that an undetected defect in expression of the WT-SCN1A allele is necessary for expression of the disease in individuals carrying single mutations (allelic imbalance). Altered balance between mutant and WT alleles has been demonstrated for certain muscle ion channel disorders (Zhou *et al.* 1994; Duno *et al.* 2004).

Structure–function correlations

Two of the mutations causing hyperpolarizing shifts in the voltage dependence of activation (V1611F and P1632S) reside within the D4 voltage-sensor domain (S3–S4 segments). Although neither of these mutations disrupt charged residues implicated directly in sensing membrane potential, replacements of valine by phenylalanine in D4/S3 or serine for proline in D4/S4 could conceivably alter voltage-dependent conformational changes of the voltage sensor. However, V983A and F1808L, which cause depolarizing and hyperpolarizing shifts in activation voltage dependence, respectively, reside outside of voltage-sensor domains in regions that lie within or adjacent to S6 segments. Rather than altering conformational responses of the voltage sensor directly, these mutations may disrupt coupling of S4 movement with activation. Studies in voltage-gated potassium channels and hyperpolarization-activated cation channels have suggested that the cytoplasmic end of S6 may participate in this coupling process through electrostatic interactions with the S4–S5 region (Tristani-Firouzi *et al.* 2002; Zhao *et al.* 2004). Similarly, experiments in a bacterial sodium channel (NaChBac) further emphasize the role of S6 in activation voltage dependence (Zhao *et al.* 2004). A possible explanation for the inactivation defect associated with F1808L is disruption of calcium binding or calcium signalling involving the proximal region of the C-terminus (Wingo *et al.* 2004), or by direct interference with the fast inactivation gate (Motoike *et al.* 2004).

Summary and conclusions

We have extensively characterized several mutations associated with ICEGTC. Our findings lead us to propose that a spectrum of sodium channel dysfunction can cause the same epilepsy syndrome rather than a predominant single mechanism. Although the molecular basis of *SCN1A*-associated epilepsy is complex, variable defects in sodium channel gating and voltage dependence underlie these disorders.

References

Abou-Khalil B, Ge Q, Desai R, Ryther R, Bazyk A, Bailey R *et al.* (2001). Partial epilepsy and generalized epilepsy with febrile seizures plus and a novel *SCN1A* mutation. *Neurology* **57**, 2265–2272.

Babitch JA & Anthony FA (1987). Grasping for calcium binding sites in sodium channels with an EF hand. *J Theor Biol* **127**, 451–459.

Bennett PB, Yazawa K, Makita N & George AL Jr (1995). Molecular mechanism for an inherited cardiac arrhythmia. *Nature* **376**, 683–685.

Cannon SC & Strittmatter SM (1993). Functional expression of sodium channel mutations identified in families with periodic paralysis. *Neuron* **10**, 317–326.

Claes L, Ceulemans B, Audenaert D, Smets K, Lofgren A, Del Favero J *et al.* (2003). De novo SCN1A mutations are a major cause of severe myoclonic epilepsy of infancy. *Hum Mutat* **21**, 615–621.

Claes L, Del Favero J, Ceulemans B, Lagae L, Van Broeckhoven C & De Jonghe P (2001). De novo mutations in the sodium-channel gene SCN1A cause severe myoclonic epilepsy of infancy. *Am J Hum Genet* **68**, 1327–1332.

Dravet C, Bureau M, Guerrini R, Giraud N & Toger J (1992). Severe myoclonic epilepsy in infants. In *Epileptic Syndromes in Infancy, Childhood and Adolescence*, ed. Rogers J, Bureau M, Dravet C, Dreifuss FE & Wolf P, pp. 75–88. John Libbey, London.

Duno M, Colding-Jorgensen E, Grunnet M, Jespersen T, Vissing J & Schwartz M (2004). Difference in allelic expression of the CLCN1 gene and the possible influence on the myotonia congenita phenotype. *Eur J Hum Genet* **12**, 738–743.

Escayg A, Heils A, MacDonald BT, Haug K, Sander T & Meisler MH (2001). A novel *SCN1A* mutation associated with generalized epilepsy with febrile seizures plus – and prevalence of variants in patients with epilepsy. *Am J Hum Genet* **68**, 866–873.

Escayg A, MacDonald BT, Meisler MH, Baulac S, Huberfeld G, An-Gourfinkel I *et al.* (2000). Mutations of SCN1A, encoding a neuronal sodium channel, in two families with GEFS+2. *Nature Genet* **24**, 343–345.

Fujiwara T, Sugawara T, Mazaki-Miyazaki E, Takahashi Y, Fukushima K, Watanabe M *et al.* (2003). Mutations of sodium channel alpha subunit type 1 (SCN1A) in intractable childhood epilepsies with frequent generalized tonic-clonic seizures. *Brain* **126**, 531–546.

Fukuma G, Oguni H, Shirasaka Y, Watanabe K, Miyajima T, Yasumoto S *et al.* (2004). Mutations of neuronal voltage-gated Na^+ channel $\alpha 1$ subunit gene *SCN1A* in core severe myoclonic epilepsy in infancy (SMEI) and in borderline SMEI (SMEB). *Epilepsia* **45**, 140–148.

Heron SE, Crossland KM, Andermann E, Phillips HA, Hall AJ, Bleasel A *et al.* (2002). Sodium-channel defects in benign familial neonatal-infantile seizures. *Lancet* **360**, 851–852.

Ito M, Nagafuji H, Okazawa H, Yamakawa K, Sugawara T, Mazaki-Miyazaki E *et al.* (2002). Autosomal dominant epilepsy with febrile seizures plus with missense mutations of the Na^+-channel $\alpha 1$ subunit gene, *SCN1A*. *Epilepsy Res* **48**, 15–23.

Kamiya K, Kaneda M, Sugawara T, Mazaki E, Okamura N, Montal M *et al.* (2004). A nonsense mutation of the sodium channel gene SCN2A in a patient with intractable epilepsy and mental decline. *J Neurosci* **24**, 2690–2698.

Lossin C, Rhodes TH, Desai RR, Vanoye CG, Wang D, Carniciu S *et al.* (2003). Epilepsy-associated dysfunction in the voltage-gated neuronal sodium channel SCN1A. *J Neurosci* **23**, 11289–11295.

Lossin C, Wang DW, Rhodes TH, Vanoye CG & George AL Jr (2002). Molecular basis of an inherited epilepsy. *Neuron* **34**, 877–884.

Motoike HK, Liu H, Glaaser IW, Yang AS, Tateyama M & Kass RS (2004). The Na^+ channel inactivation gate is a molecular complex: a novel role of the COOH-terminal domain. *J Gen Physiol* **123**, 155–165.

Ohmori I, Ouchida M, Ohtsuka Y, Oka E & Shimizu K (2002). Significant correlation of the SCN1A mutations and severe myoclonic epilepsy in infancy. *Biochem Biophys Res Commun* **295**, 17–23.

Rhodes TH, Lossin C, Vanoye CG, Wang DW & George AL Jr (2004). Noninactivating voltage-gated sodium channels in severe myoclonic epilepsy of infancy. *Proc Natl Acad Sci U S A* **101**, 11147–11152.

Scheffer IE, Wallace R, Mulley JC & Berkovic SF (2001). Clinical and molecular genetics of myoclonic-astatic epilepsy and severe myoclonic epilepsy in infancy (Dravet syndrome). *Brain Dev* **23**, 732–735.

Spampanato J, Escayg A, Meisler MH & Goldin AL (2001). Functional effects of two voltage-gated sodium channel mutations that cause generalized epilepsy with febrile seizures plus type 2. *J Neurosci* **21**, 7481–7490.

Spampanato J, Escayg A, Meisler MH & Goldin AL (2003). Generalized epilepsy with febrile seizures plus type 2 mutation W1204R alters voltage-dependent gating of $Na_V1.1$ sodium channels. *Neuroscience* **116**, 37–48.

Spampanato J, Kearney JA, de Haan G, McEwen DP, Escayg A, Aradi I *et al.* (2004). A novel epilepsy mutation in the sodium channel SCN1A identifies a cytoplasmic domain for beta subunit interaction. *J Neurosci* **24**, 10022–10034.

Sugawara T, Mazaki-Miyazaki E, Fukushima K, Shimomura J, Fujiwara T, Hamano S *et al.* (2002). Frequent mutations of SCN1A in severe myoclonic epilepsy in infancy. *Neurology* **58**, 1122–1124.

Sugawara T, Mazaki-Miyazaki E, Ito M, Nagafuji H, Fukuma G, Mitsudome A *et al.* (2001*a*). $Na_V1.1$ mutations cause febrile seizures associated with afebrile partial seizures. *Neurology* **57**, 703–705.

Sugawara T, Tsurubuchi Y, Agarwala KL, Ito M, Fukuma G, Mazaki-Miyazaki E *et al.* (2001*b*). A missense mutation of the Na^+ channel α_{II} subunit gene $Na_V1.2$ in a patient with febrile and afebrile seizures causes channel dysfunction. *Proc Natl Acad Sci U S A* **98**, 6384–6389.

Sugawara T, Tsurubuchi Y, Fujiwara T, Mazaki-Miyazaki E, Nagata K, Montal M *et al.* (2003). $Na_V1.1$ channels with mutations of severe myoclonic epilepsy in infancy display attenuated currents. *Epilepsy Res* **54**, 201–207.

Tristani-Firouzi M, Chen J & Sanguinetti MC (2002). Interactions between S4–S5 linker and S6 transmembrane domain modulate gating of HERG K^+ channels. *J Biol Chem* **277**, 18994–19000.

Wallace RH, Scheffer IE, Barnett S, Richards M, Dibbens L, Desai RR *et al.* (2001). Neuronal sodium-channel $\alpha 1$-subunit mutations in generalized epilepsy with febrile seizures plus. *Am J Hum Genet* **68**, 859–865.

Wallace RH, Wang DW, Singh R, Scheffer IE, George AL Jr, Phillips HA *et al.* (1998). Febrile seizures and generalized epilepsy associated with a mutation in the Na^+-channel $\beta 1$ subunit gene, *SCN1B*. *Nature Genet* **19**, 366–370.

Wingo TL, Shah VN, Anderson ME, Lybrand TP, Chazin WJ & Balser JR (2004). An EF-hand in the sodium channel couples intracellular calcium to cardiac excitability. *Nature Struct Mol Biol* **11**, 219–225.

Yamakawa K (2005). Epilepsy and sodium channel gene mutations: gain or loss of function? *Neuroreport* **16**, 1–3.

Zhao Y, Scheuer T & Catterall WA (2004). Reversed voltage-dependent gating of a bacterial sodium channel with proline substitutions in the S6 transmembrane segment. *Proc Natl Acad Sci U S A* **101**, 17873–17878.

Zhou J, Spier SJ, Beech J & Hoffman EP (1994). Pathophysiology of sodium channelopathies: correlation of normal/mutant mRNA ratios with clinical phenotype in dominantly inherited periodic paralysis. *Hum Mol Genet* **3**, 1599–1603.

Acknowledgements

This project was supported in part by a grant from the RIKEN Brain Science Institute (I. Ogiwara, K.Y.) and by NIH grant NS32387 (A.L.G.).